Isotope effect in dissociative electron attachment to HCN

S. T. Chourou and A. E. Orel

Isotope effect in dissociative electron attachment to HCN

S. T. Chourou[1] and A. E. Orel[1]

[1]Department of Applied Science, University of California, Davis, Davis CA 95616 USA*

Abstract

We performed nuclear dynamics calculations on HCN and DCN to study the isotope effect in dissociative electron attachment (DEA). Our previous calculations at 333 K led to a ratio $\sigma^{(CN^-/HCN)}/\sigma^{(CN^-/DCN)}$ of about 13 which is significantly higher than recent experimental findings. This discrepancy is attributed to the neglect of correlation and polarization effects in the scattering calculation performed. We carried out a relaxed-SCF calculation to determine the variation of the resonance parameters under these effects. We observe a shift in the positions of the shape resonance as well as a narrowing of the autoionization widths resulting in an isotope ratio of 3.2 at T = 333 K; in closer agreement with the measured value.

*Electronic address: stchourou@ucdavis.edu

I. INTRODUCTION

Recently, May *et al.* conducted a time-of-flight ion spectrometry experiment to measure the isotope effect in DEA to HCN [1]. The authors measured a $\sigma^{(CN^-/HCN)}/\sigma^{(CN^-/DCN)}$ ratio of 2.76 at 333 K below 3 eV in electron energy. Previous theoretical work on DEA to HCN shows a value of 13 for this ratio [2]. It has been speculated that this discrepancy is due to the significant sensitivity of the wavepacket flux to the computed values of the autoionization widths. In order to test this hypothesis, we have carried out a more accurate electron scattering calculation that includes the polarization and correlation effects. We then performed a new 3-D wavepacket propagation run using the improved complex adiabatic potential energy surface (APES) in the A' symmetry. In this paper, we first give a brief overview of the relaxed-SCF approach used in this study and discuss the results of the electron scattering calculation. Secondly, we describe the results of the nuclear dynamics calculation and compare the DEA cross section of HCN and DCN to experimental findings.

II. BACKGROUND

Here we review the method employed to solve for the dissociation dynamics of the tri-atomic system. We have represented the internal degrees of freedom using the Jacobi coordinates $\mathbf{Q} = (r, R, \theta)$ as show in Fig.(1).

The nuclear dynamics of the metastable negative ion state is expressed within the local potential approximation [3] to give the nuclear wave equation:

$$\left[E_{tot} - \hat{T}_Q - E_{el}(\mathbf{Q}) - \epsilon_{res}(\mathbf{Q}) + \frac{i}{2}\Gamma(\mathbf{Q}) \right] \xi_{nuc}(\mathbf{Q}) = \left(\frac{\Gamma(\mathbf{Q})}{2\pi} \right)^{1/2} \chi_\nu(\mathbf{Q}) \tag{1}$$

where E_{tot} is the total energy of the {electron, molecule} system, E_{el} represents the ground electronic state of the neutral, ϵ_{res} is the resonance energy and Γ is the autoionization width within the Local Complex Potential model [4]. The latter three functions are expressed as a function of $\mathbf{Q}$ to form the 3-D anion complex potential energy surfaces. In Eq.(1), ξ_{nuc} represents the nuclear wave function and χ_ν the initial vibrational state of the neutral target.

Here, the kinetic energy operator $\hat{T}_Q$ is given for a total momentum operator $J = 0$ and is expressed in the Jacobi coordinates as
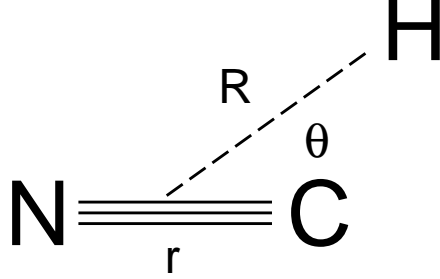
Figure 1: (Color online) Molecule in Jacobi coordinates.

$$\hat{T}_Q = -\frac{1}{2\mu_r}\partial_r^2 - \frac{1}{2\mu_R}\partial_R^2 - \frac{1}{2}\left(\frac{1}{\mu_r r^2} + \frac{1}{\mu_R R^2}\right)\frac{1}{\sin\theta}\partial_\theta(\sin\theta\ \partial_\theta), \tag{2}$$

where μ_r and μ_R specify the reduced masses associated with the r and R coordinates (Note that atomic units $\hbar = m = 1$ are used).

We further use the time-dependent formulation of this wave equation as established by McCurdy and Turner [5] to compute the DEA wavefunction $\Phi_{nuc}(\mathbf{Q}, t)$. The working equation of motion is therefore given by

$$\begin{cases} \left[\hat{T}_Q + E_{el}(\mathbf{Q}) + \epsilon_{res}(\mathbf{Q}) - \frac{i}{2}\Gamma(\mathbf{Q})\right]\Phi_{nuc}(\mathbf{Q}, t) = i\partial_t\Phi_{nuc}(\mathbf{Q}, t); \\ \Phi_{nuc}(\mathbf{Q}, 0) = \left(\frac{\Gamma(\mathbf{Q})}{2\pi}\right)^{1/2}\chi_\nu(\mathbf{Q}) \end{cases} \tag{3}$$

We use the computational technique based on Multi-Configuration Time-Dependant Hartree (MCTDH) formalism discussed in detail in [6]. In this approach, the nuclear wave function for the negative ion is expressed in the Jacobi coordinates as:

$$\Phi_{nuc}(r, R, \theta, t) = \sum_{i=1}^{N_r}\sum_{j=1}^{N_R}\sum_{k=1}^{N_\theta} A_{ijk}(t)\rho_i(r, t)\varrho_j(R, t)\Theta_k(\theta, t) \tag{4}$$

3

Each single-particle function appearing in Eq.(4) is in turn expanded in terms of a function basis set chosen to correspond to that of a Discrete Variable Representation (DVR) for computational efficiency. Here, N_r, N_R and N_θ are all set to the value 8 and the single-particle functions associated with the variables R, r and θ are expressed in terms of sine-DVR (99 grid points), Harmonic Oscillator-DVR (27 grid points) and Legendre-DVR (121 grid points) respectively.

III.   COMPLEX APES

Our previous scattering calculation in [2] was conducted at the static exchange level. In this case, the expression of the trial electronic wavefunction is given by [7]

$$\phi_\lambda^+(\mathbf{r}; \mathbf{q}) = \sum_{\lambda'} \mathcal{A} \left[\varphi_{\lambda'}(\vec{r}_1, \vec{r}_2, ..., \vec{r}_n; \mathbf{q}) F^{\lambda\lambda'}(\vec{r}_{n+1}; k_\lambda) \right], \tag{5}$$

where the sum runs over the energetically open n-electron target states, $\mathbf{r} = (\vec{r}_1, \vec{r}_2, ..., \vec{r}_{n+1})$ is the $(n+1)$-electronic coordinates vector, $\mathcal{A}$ is the antisymmetrizing operator and the label λ groups all the quantum numbers needed to represent the physical state of the {electron, molecule} system i.e. the internal state of the target and the energy and orbital angular momentum of the scattered electron. The function $\varphi_\lambda(\vec{r}_1, \vec{r}_2, ..., \vec{r}_n; \mathbf{q})$ in Eq.(5) is the target n-electron ground state with the nuclei clamped at $\mathbf{q}$ and $F^{\lambda\lambda'}(\vec{r}_{n+1}; k_\lambda)$ is the one-electron scattering wavefunction as a function of the electron's position $\vec{r}_{n+1}$ and momentum k_λ. This level of approximation does not take into account polarization and correlation effects of the {electron, molecule}. In the current work, the scattering wavefunction used in given by

$$\phi_\lambda^+(\mathbf{r}; \mathbf{q}) = \sum_{\lambda'} \mathcal{A} \left[\varphi_{\lambda'}(\vec{r}_1, \vec{r}_2, ..., \vec{r}_n; \mathbf{q}) F^{\lambda\lambda'}(\vec{r}_{n+1}; k_\lambda) \right] + \sum_\mu d_\mu^\lambda \Theta_\mu(\mathbf{r}), \tag{6}$$

where the additional expansion involves an orthonormal set $\{\Theta_\mu\}_\mu$ of antisymmetric, square-integrable $(n+1)-$electron functions and represents the polarization and correlation effects not contained in the first summation .

In this relaxed-SCF calculation, we have used a basis set of 66 functions allowing symmetry-preserving excitations from occupied HCN orbitals into virtual orbitals resulting in 9405 configurations in the A' symmetry. Fig.(2) shows the eigenphase sums obtained

for various molecular geometries and compares the fitted resonance parameters to previous static exchange calculation of [2]. As expected, inclusion of the correlation and polarization term in Eq.(6) leads to a shift of the resonance positions to lower energies and to a narrowing of the autoionization widths. For instance, at quasi-equilibrium geometry ($1°$ bend), we observe a decrease of the lower resonance energy by about 0.04 a.u. (i.e. around 36.3%
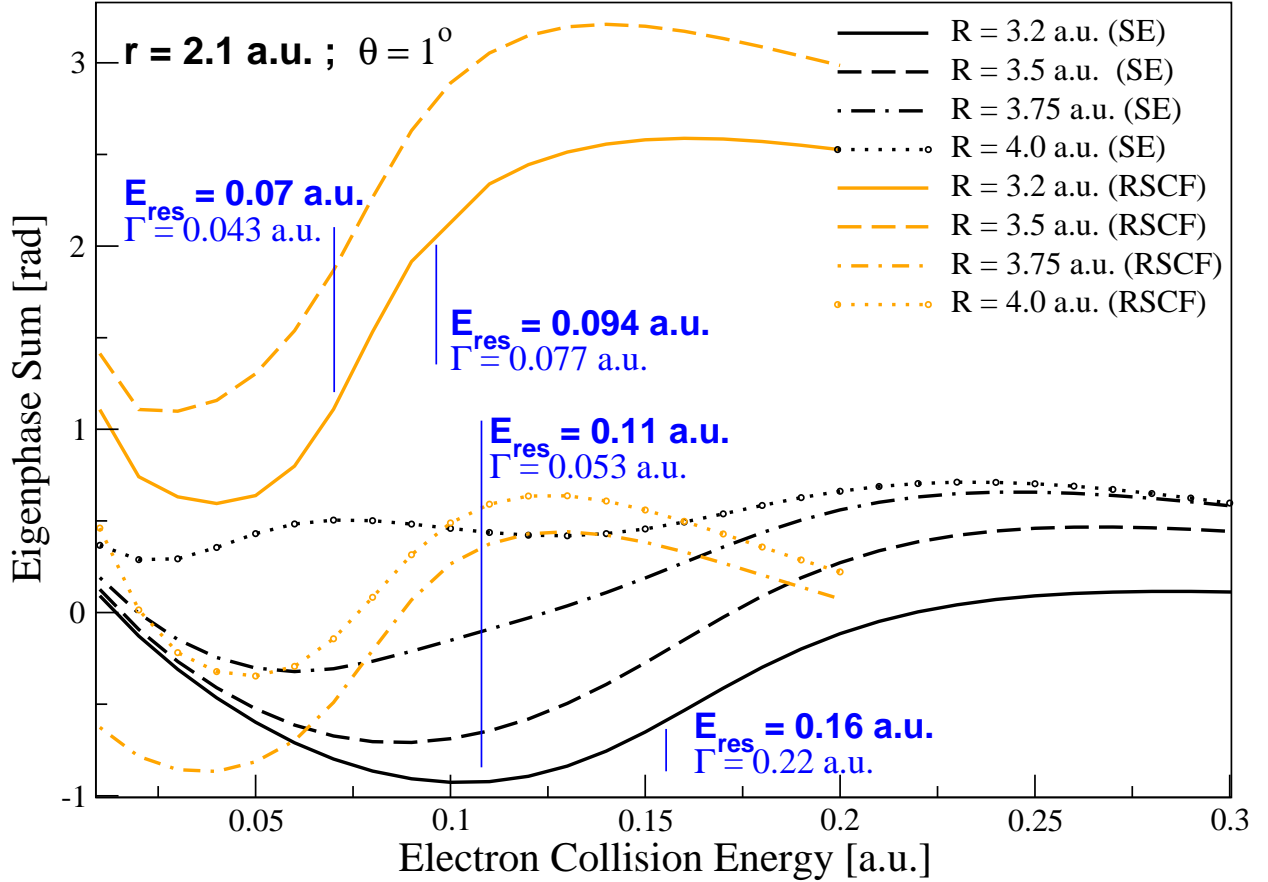

Figure 2: (Color online) Eigenphase sums as a function of electron collision energy with variations in R with $r = 2.1$ a.u. and $\theta = 1°$. The resonance parameters for (overlapping) resonances are shown for the quasi-equilibrium geometry $R = 3.2$ a.u.

Fig.(4) depicts the shape of the lowest resonant potential energy surface constructed based on this calculation as a function of the internal degrees of freedom of HCN. In Fig.(5), the correspondent imaginary part of the complex potential surface Γ is plotted as a function of the coordinates R and θ. Qualitatively, these surfaces bear a great topological resemblance
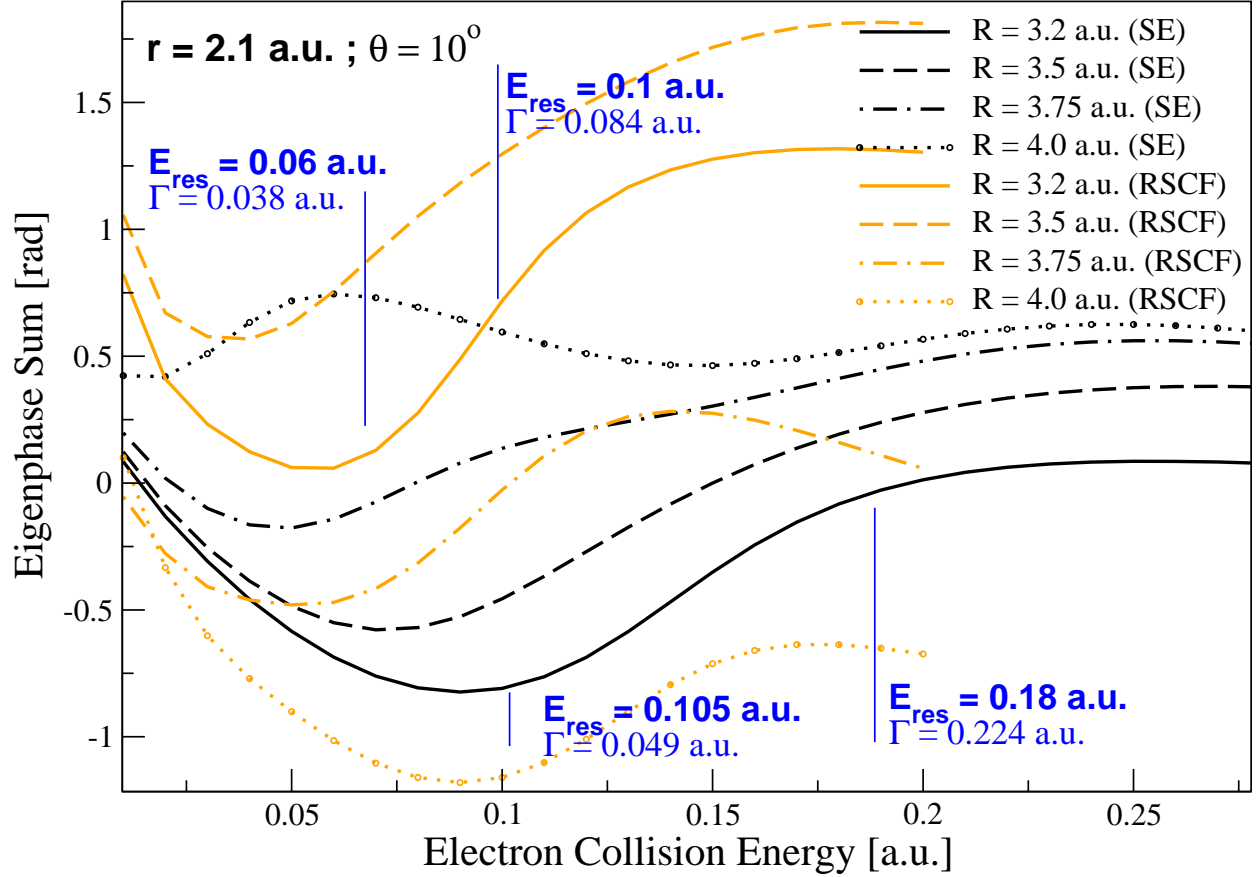
Figure 3: (Color online) Eigenphase sums as a function of electron collision energy with variations in R with $r = 2.1$ a.u. and $\theta = 10°$. The resonance parameters for (overlapping) resonances are shown for the quasi-equilibrium geometry $R = 3.2$ a.u.

to the ones obtained in our previous work. However, the changes in the values of the resonance parameters cause a variation in the relative neutral-anion surface position (and hence, the position and shape of the curve crossing seam) as well as the width and height of the potential barrier that characterizes this A' APES.

IV.   DEA CROSS SECTION

In the framework of the local complex potential model [4] used to describe to nuclear motion, the propagating wavepacket undergoes the effect of the $\Gamma(\mathbf{q})$ function both through the initial condition (or the driving term of the wave equation) and the complex potential expressed in the Hamiltonian operator. The nuclear motion is computed using Multi-
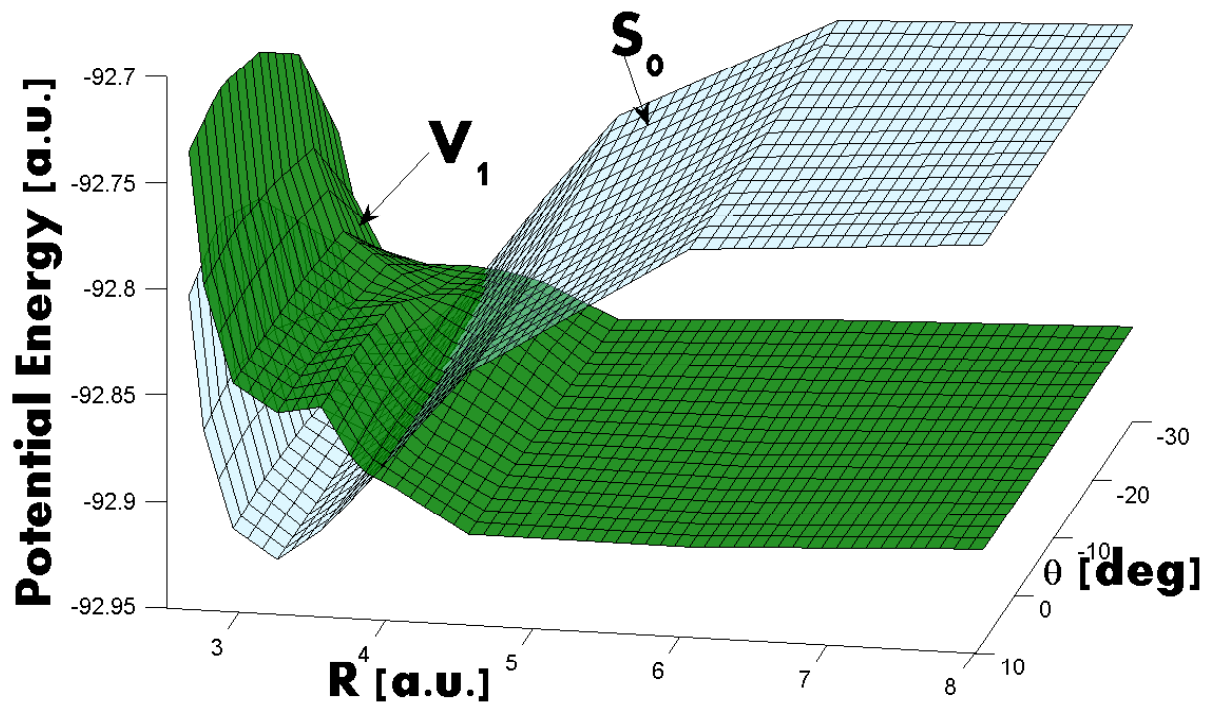
Figure 4: (Color online) 3-D plots of the ground electronic state of the HCN target (S_0) and of the lowest resonant APES (real part (V_1)) of HCN^{-*}. Surfaces are shown as a function of the Jacobi coordinates R and θ where the latter is shown within the interval $[-30°, 10°]$. The plot shows the crossing of the resonant anion and neutral states and the potential barrier observed in the resonant surface. The cut at $10°$ depicts the surface profiles along the dissociative coordinate R.

Configuration Time-Dependent Hartree approach using the Heidelberg Package [6] to compute the propagation of each of the 4 low-lying bending vibrational states for HCN. The excited states used are obtained by applying successively an angular raising operator on the ground vibrational mode.

This set of individual vibrational modes cross sections were combined using a weight given by a Boltzmann distribution at 333 K to calculate the total contribution to the DEA cross section. The resulting partial DEA cross sections and the population-weighted sums
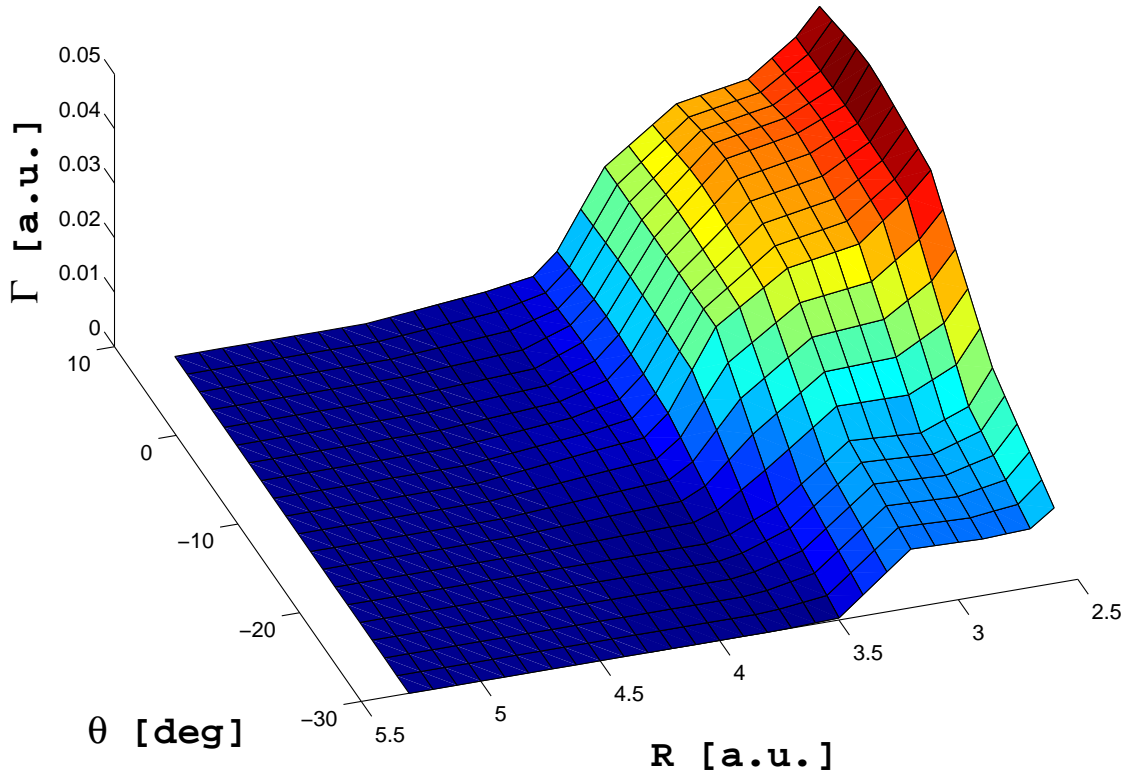
Figure 5: (Color online)3-D plots of the imaginary part Γ of lowest resonant APES of HCN^{-*}. The surface is shown as a function of the Jacobi coordinates R and θ where the latter is shown within the interval $[-30°, 10°]$.

are shown in Fig.(6) and Fig.(7) respectively for HCN and DCN. In these figures further compare the present results to the experimental values of May *et al.* [1].

The theoretical plots are in good agreement with the experiment in terms of DEA peak positions, heights and widths. The calculated DEA cross sections are centered approximately around 1.94 eV with a maximum value of 865.6 pm^2 for HCN and 283.1 pm^2 for DCN. Furthermore, the FWHM of the calculated cross sections are evaluated at 0.77 eV and 0.68 eV for HCN and DCN respectively. This calculation results in a value of the $\sigma^{(CN^-/HCN)}/\sigma^{(CN^-/DCN)}$ ratio at 1.94 eV of approximately 3.05 in close agreement with the experimental 2.76 value. These values are summarized in Table I and Table II respectively for HCN and HCN.
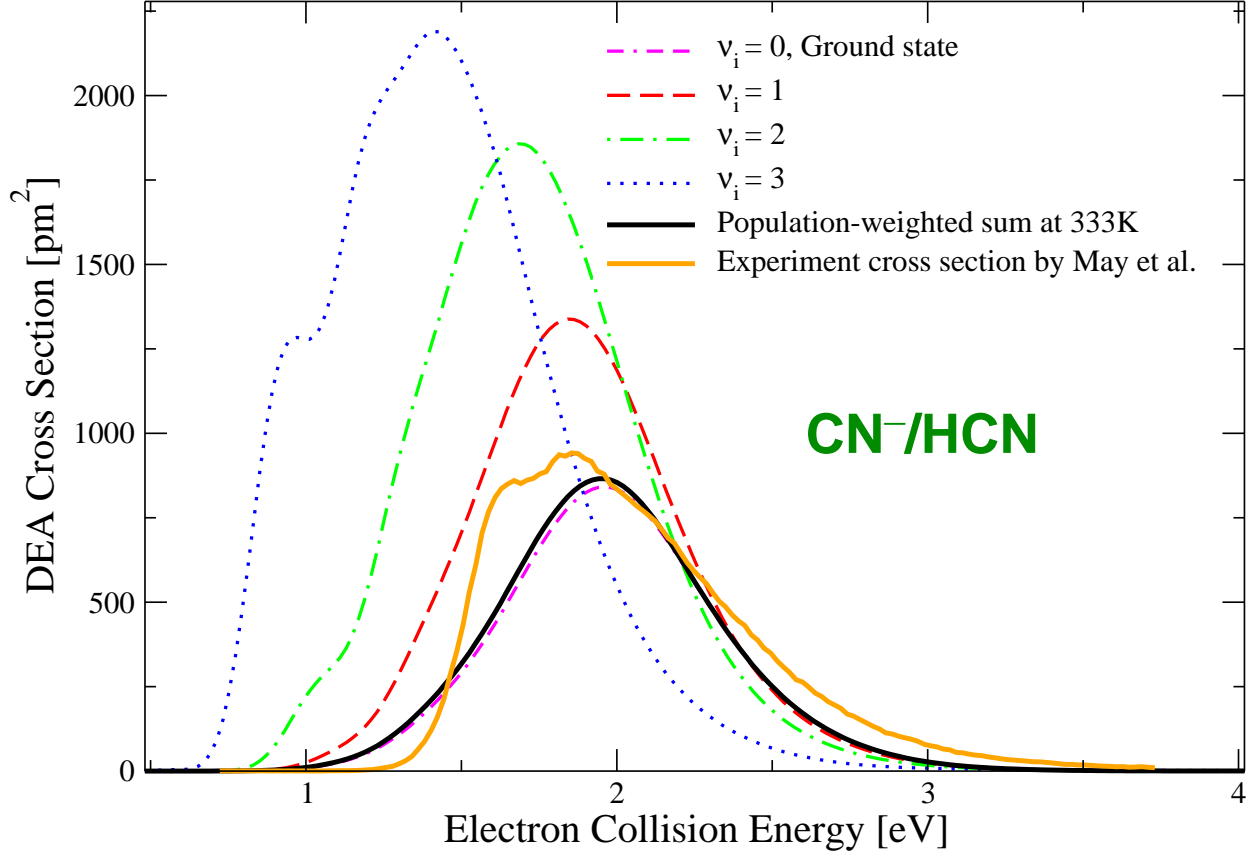
Figure 6: (Color online) Absolute DEA cross section for initial HCN vibrational states $\nu_i = 0$, 1, 2 and 3 and the population-weighted sum at 333 K. Comparison with DEA cross section in [1] is shown in the solid orange plot.

Table I: Comparative summary of DEA cross section characteristics for HCN

	Experiment[1]	Previous work[2]	Present work
Peak max. position (eV)	1.85	3.01	1.94
Peak height (pm^2)	942	2790	865.6
FWHM (eV)	0.84	1.6	0.77

However, we note that this calculation only shows a modest agreement with experiment in terms of the DEA peak onsets and the secondary shoulder feature in May *et al.*'s measurements. The authors attributed this feature to the contribution of the ground and excited
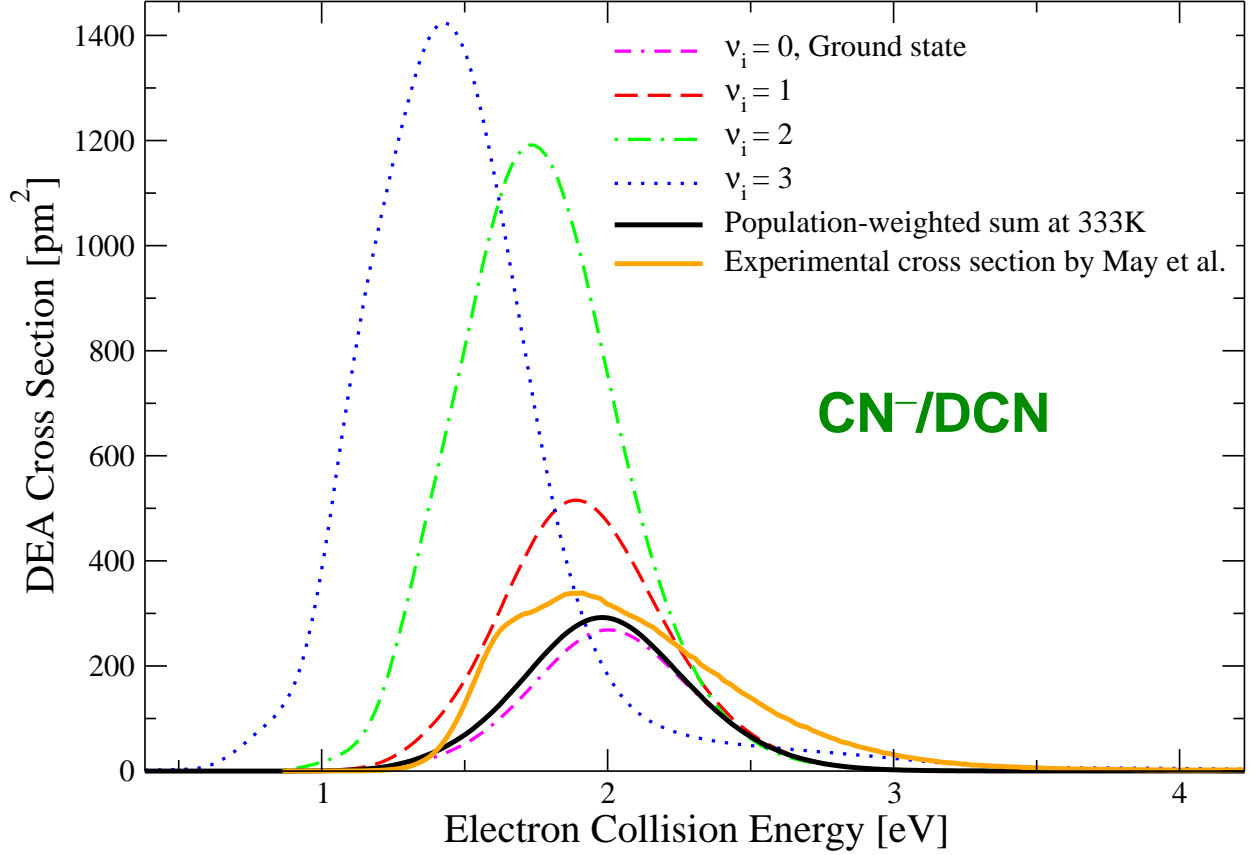
Figure 7: (Color online) Absolute DEA cross section for initial DCN vibrational states $\nu_i = 0$, 1, 2 and 3 and the population-weighted sum at 333 K. Comparison with DEA cross section in [1] is shown in the solid orange plot.

Table II: Comparative summary of DEA cross section characteristics for DCN

	Experiment[1]	Previous work[2]	Present work
Peak max. position (eV)	1.91	3.18	1.94
Peak height (pm^2)	339	215	283.1
FWHM (eV)	0.88	1.9	0.68

vibrational states of the dissociated CN^- fragment. We carried out a projection of the asymptotic state of the resonant anion onto the vibrational states ν_0, ν_1, ν_2, and ν_3 of the CN^- fragment. Fig.(8) and Fig.(9) show a plot of the cross section associated with each of the fragment vibrational states in the case of HCN and DCN respectively. The peak height ratios are found to be 1, 0.3, 0.09 and 0.017 (1, 0.2, 0.05 and 4×10^3) for HCN (DCN) for the CN^- vibrational states ν_0, ν_1, ν_2, and ν_3 respectfully.

10

Figure 8: (Color online) Cross sections for final CN^- vibrational states ν_0, ν_1, ν_2 and ν_3 for HCN.

V. CONCLUSION

A relaxed-SCF calculation is necessary to obtain a more accurate treatment of dynamics of HCN and DCN. The inclusion of the polarization and correlation effects provides a better description of the interaction between the incident electron and the neutral target and thus, leads to a better agreement with experimental results. This is consistent with the assumption that the DEA cross section is significantly sensitive to the resonance parameters. This improved calculation further results in a good agreement for the $\sigma^{(CN^-/HCN)}/\sigma^{(CN^-/DCN)}$ ratio which indicates that the relaxed-SCF calculation yields a more accurate topology of the complex potential used in the nuclear wave equation for HCN and DCN.

Examination of the experimental cross section in [1] shows a double peak structure where the lowest and smallest of the peaks lies at about 0.2 eV below the main peak for both HCN and DCN. The authors attribute this feature to possible contribution from the excited vibrational states of CN^-. This feature is not present in our current calculation where
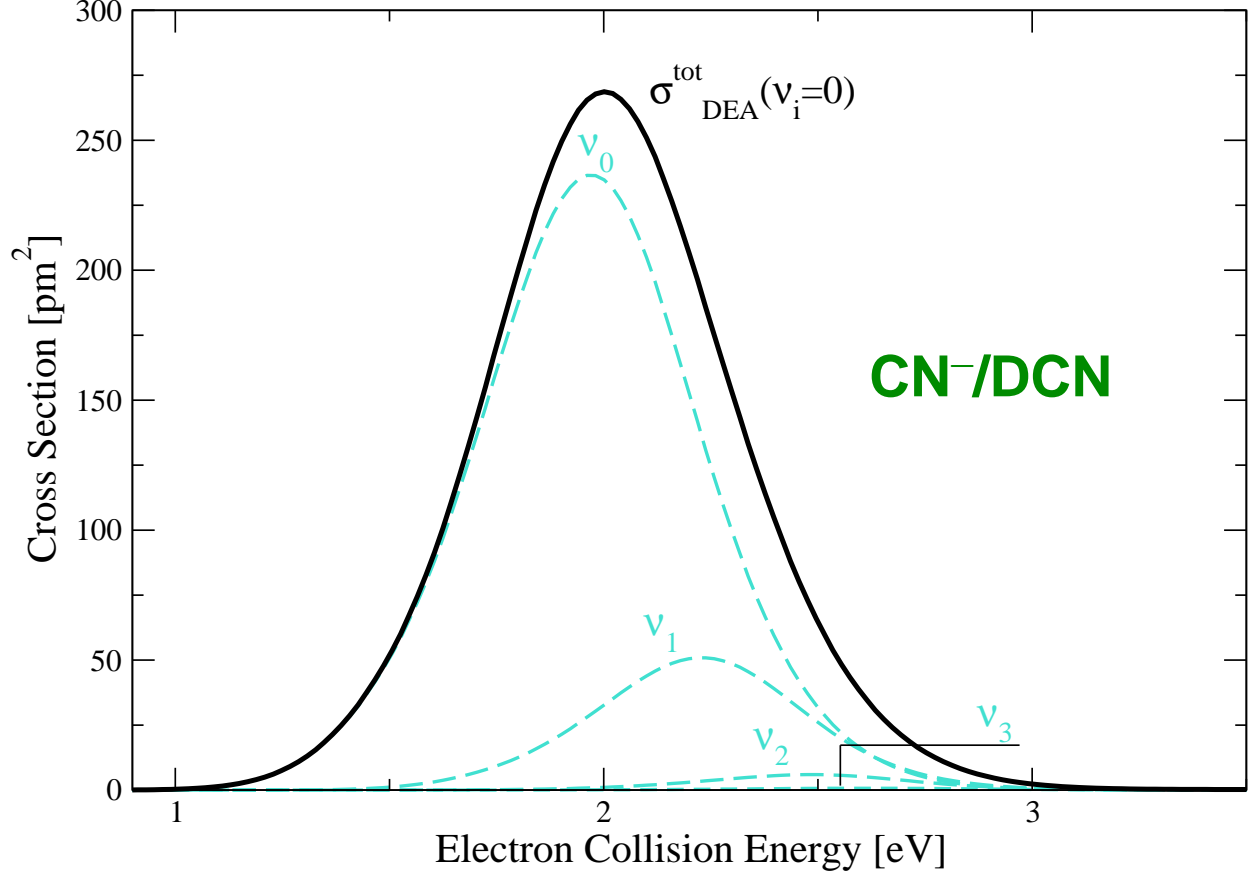
11

Figure 9: (Color online) Cross sections for final CN^- vibrational states ν_0, ν_1, ν_2 and ν_3 for DCN.

only a single peak structure consistent with the main experimental peak is observed. The double-peak structure may be the result of a coupling to a higher resonant state where non-adiabatic coupling terms introduce interference effects in the propagating wavepacket as seen in cases elsewhere [8]. In fact, as detailed in [2], the 2 complex adiabatic surfaces of HCN intersect at the crossing point of $^2\Sigma$ and $^2\Pi$ resonant states in linear geometry. The present computation, however, neglects the vibronic interaction between these states which may explain the absence of the minor peak observed experimentally. The inclusion of coupling between the resonant states entails a computationally complicated diabatization procedure to determine the non-adiabatic matrix elements and the solution of a system of two coupled wave equations of the tridimensional HCN and DCN systems. This calculation goes beyond the scope of the present study.

---

[1] O. May, D. Kubala, and M. Allan, Phys. Rev. A **82**, 010701 (2010)

[2] S. T. Chourou and A. E. Orel, Phys. Rev. A **80**, 032709 (2009)

[3] A. U. Hazi, T. N. Rescigno, and M. Kurilla, Phys. Rev. A **23**, 1089 (1981)

[4] A.U. Hazi, T.N. Rescigno, and M. Kurilla, Phys. Rev. A **23**, 1089 (1981)

[5] C. W. Mcurdy and J. L. Turner, J. Chem. Phys. **78**, No. 11, (1983)

[6] G. A. Worth, M. H. Beck, A. Jackle, and H.-D. Meyer, MCTDH package, Version 8.4 (2007); See *http://www.pci.uni-heidelberg.de/tc/usr/mctdh/*

[7] T.N. Rescigno, C.W. McCurdy, A.E. Orel and B.H. Lengsfield,III, "The Complex Kohn Variational Method", Proceedings of the Workshop on Comparative Study of Current Methodologies in Electron-Molecule Scattering, ISBN 0-306-44911-0 (1993)

[8] J. B. Roos, M. Larsson, and A. Larson and A. E. Orel, Phys. Rev. A **80**, 012501 (2009)